LIMNOLOGY AND OCEANOGRAPHY
Letters

ASLO
Open Access

Limnology and Oceanography Letters 5, 2020, 264–270

doi: 10.1002/lol2.10139

LETTER

Storm-induced turbulence alters shelf sea vertical fluxes

Larissa K. P. Schultze ,* *Lucas M. Merckelbach, Jeffrey R. Carpenter*
Institute of Coastal Research, Helmholtz-Zentrum Geesthacht, Geesthacht, Germany

Scientific Significance Statement

Summer storms are able to disturb stratification in the water column and bring up nutrients to the sunlit region, supporting primary productivity. These abrupt physical and ecosystem changes are initiated by elevated levels of storm-driven ocean turbulence; yet despite the crucial role played by turbulence, there is a paucity of observations due to measurement difficulties during such extreme conditions. Overcoming the measurement difficulties, this study shows that the vertical turbulent transport of scalars is significantly increased by nearly an order of magnitude during storm events, and estimates that storms could contribute to 40% of the fluxes across a stratified water column during summer, thus indicating that storm events could potentially have a significant influence on the biogeochemistry of the shelf seas.

Abstract

Storms are infrequent, intense, physical forcing events that represent a potentially significant driver of ocean ecosystems. The objective of this study was to assess changes in water column structure and turbulent fluxes caused by storms using an autonomous underwater glider, as well as the chlorophyll *a* (Chl *a*) response to the altered physical environment. The glider was able to measure throughout the complete life cycle of Storm Bertha as it passed over the North Sea in August 2014, from its arrival to dissipation. Storm Bertha triggered rapid mixing of the thermocline through shear instability, increasing vertical fluxes by nearly an order of magnitude, and promoting increases in surface layer Chl *a*. The results demonstrate that storms represent a significant fraction of seasonal vertical turbulent fluxes, with potentially important consequences for biological production in shelf seas.

An increase in the frequency and strength of storms over the North Sea is one of the predicted consequences of a changing climate system (Feser et al. 2015). Because shelf seas, such as the North Sea, have a disproportionately high influence on global biological production (Simpson and Sharples 2012), the response of these ecosystems to storm events must be understood in order to predict future alterations. For example, storm-enhanced mixing is expected to bring an overall elevated amount of nutrients to the sunlit region of the water column, possibly supporting primary production (van Beusekom and Diel-Christiansen 2009; Rumyantseva et al. 2015). Additionally, fall storms have shown to increase the CO_2 uptake from the atmosphere as a result of the deepening of the surface mixed layer (Thomas et al. 2004). Finally, understanding rapid sea surface temperature changes caused by enhanced thermocline mixing as a result of elevated wind speeds has been found to

*Correspondence: larissa.schultze@hzg.de

Associate editor: Peter Franks

Author Contribution Statement: LKPS, JRC, and LMM came up with the research question and designed the study approach. JRC and LMM designed the field survey and collected the field measurements. LKPS and JRC conducted the data analyses. LKPS and JRC wrote the paper.

Data Availability Statement: The glider data, the processed shear microstructure and the ADCP data, and the respective metadata are available in the Zenodo repository at https://doi.org/10.5281/zenodo.3525787. The wind data are available in the FINO repository at http://fino.bsh.de/.

be crucial to improve forecasts on the evolution of tropical cyclones (Glenn et al. 2016).

The role of enhanced wind forcing by storms in replenishing nutrients in the euphotic zone and supporting primary production has recently gained increased attention in an attempt to improve understanding of the physical processes supporting the biological food chain (Babin et al. 2004; Rumyantseva et al. 2015). While evidence for an increase in phytoplankton concentration has been found through satellite observations (Babin et al. 2004), the intensification of turbulent fluxes during storms has never been directly assessed due to constraints in measurement capabilities under adverse weather conditions (Rumyantseva et al. 2015). Moreover, the significance of summer storm events on the seasonal budget of nutrients and on biological productivity has yet to be estimated.

In this study, we use an autonomous underwater glider equipped with a microstructure package that enables turbulence measurements under adverse weather conditions; an experiment made possible through recent technological development in this field of research. The glider was used to analyze changes in water column structure caused by Storm Bertha as it passed over the German Bight region of the North Sea in summer 2014 (Fig. 1). More specifically, we address how vertical turbulent fluxes change under such an extreme weather event and how they affect stratification and chlorophyll *a* (Chl *a*) fluorescence across the water column. Furthermore, the study aimed at advancing our understanding of the physical mechanisms of storm-driven turbulent mixing, and quantifying the potential importance of storms in influencing biological activity in shelf seas over seasonal time scales.

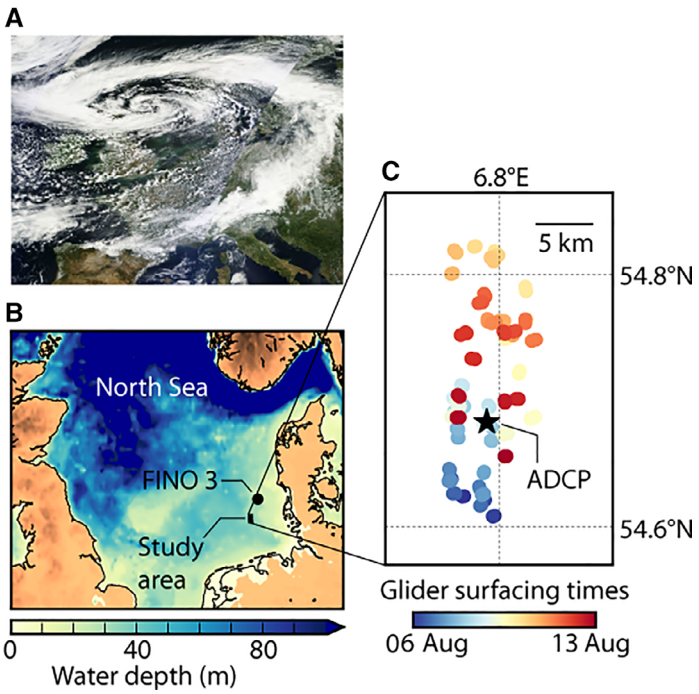

Fig. 1. Storm Bertha and the North Sea study area. (A) True color satellite image of Storm Bertha as it passes over the North Sea at times between 09:40 and 11:25 UTC on 11 August 2014 (from NASA Worldview). (B) Topography of the North Sea showing the location of the study area and the FINO 3 research station where the wind measurements were recorded. (C) Glider surfacing positions during the campaign, with times represented by colors. The position on the sea-bed of the acoustic Doppler current profiler (ADCP), used to measure water velocities, is indicated by the black star.

Materials and methods

Description of the experiment

A Teledyne Webb Research Slocum Electric autonomous underwater glider sampled between 54.61°N, 6.72°E and 54.82°N, 6.85°E in the period of 06 August to 13 August, and remained within a 17.5 km radius from an acoustic Doppler current profiler (ADCP) moored to the sea bed (Fig. 1). Furthermore, it remained within 45–70 km distance from the measurement platform FINO3, located at 55.19°N, 7.15°E, from which we have obtained wind speed data (http://fino.bsh.de).

Glider-based measurements

The glider was equipped with a Seabird free flush conductivity, temperature and depth sensor (Seabird SBE41 CTD, 0.5 Hz), and a Wetlabs FLNTU fluorescence optical sensor (1 Hz) (Schultze et al. 2019). The CTD measurements were used to calculate conservative temperature, buoyancy frequency squared (N^2), and in the identification of the thermocline boundaries. Density was calculated as described in Schultze et al. (2017). Additionally, the glider carried a navigation pressure sensor, an attitude sensor, an altimeter, an Iridium modem, and a global positioning system. The direct quantification of the dissipation rate of turbulent kinetic energy ε was enabled by mounting a microstructure package (MicroRider-1000LP, Rockland Scientific International) carrying two shear microstructure sensors (SPM – 38, 512 Hz) on the glider (Fer et al. 2014; Schultze et al. 2017, 2019), following the general methods extensively described in Lueck et al. (2002), Wolk et al. (2002), and Fer et al. (2014). A full description of the steps to determine ε, and the steps taken to control the quality of glider-based measurements, are found in Schultze et al. (2017).

Until 10 August, a special strategy for the collection of glider data was used, the "spiral missions." In the spiral missions, the tail rudder position of the glider is fixed, such that the glider profiles the water column in a spiral fashion. This flight pattern was chosen to produce measurements that are as close to Lagrangian as possible. Furthermore, the missions typically result in low spatial variability, which enables the assessment of the temporal development of fluid properties (Schultze et al. 2017). On 10 August, however, the glider was drifting northwards outside the study region as a result of elevated current speeds, such that the spiral missions had to be

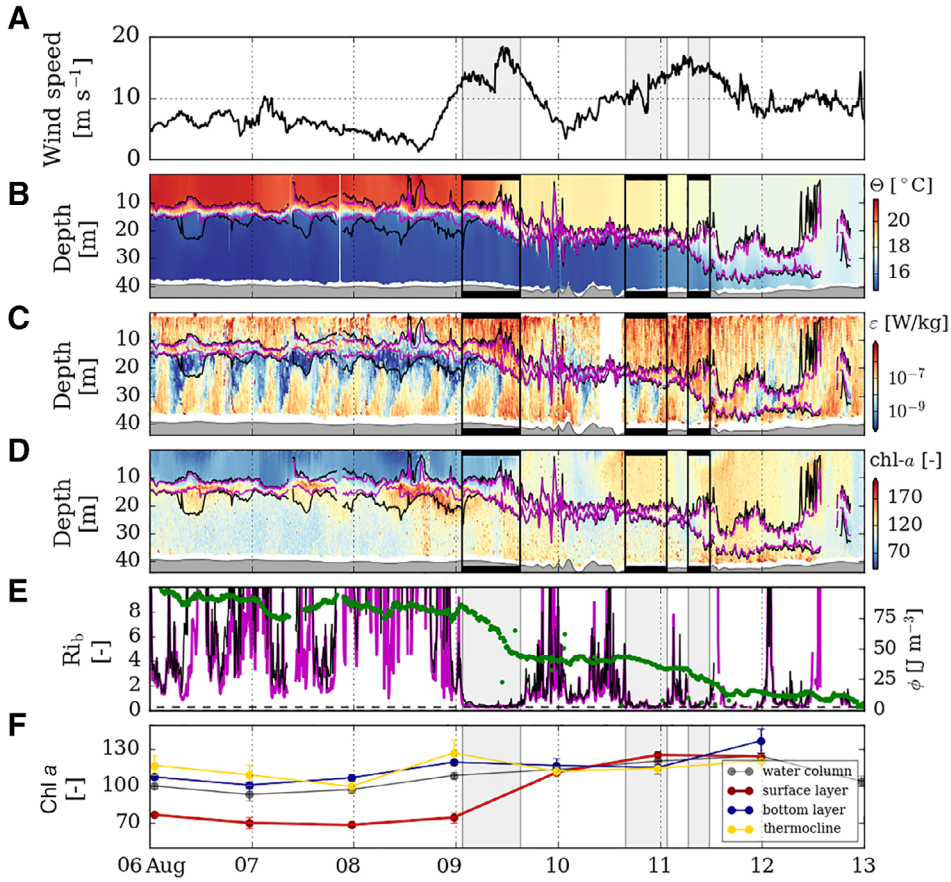

Fig. 2. Time series of storm forcing and the physical and biological response. Each panel represents (A) wind speed at 10 m height, (B) water temperature, (C) turbulent dissipation rate, (D) Chl *a* fluorescence in relative units, (E) bulk Richardson number calculated using the 90%- (black line) and the 80%-thermocline (magenta line) definitions, and the stratification index (ϕ, in green), and (F) mean Chl *a* fluorescence in the water column (gray), thermocline (yellow), bottom mixed layer (blue), and surface mixed layer (red). To avoid quenching effects, only nighttime Chl *a* measurements were taken into consideration in the calculation of mean values. In panels (B–D), the upper and lower boundaries of the stratified thermoclines are indicated by the thin magenta (80%-thermocline) and black lines (90%-thermocline), with the gray area indicating the sea bed. In each panel, the times indicated by the dark rectangles (B–D), or gray shaded rectangles (A, E, F), correspond to periods of marginal thermocline stability.

interrupted, and the glider was brought back in the vicinity of the ADCP, which is described below (cf. Fig. 1).

ADCP data

Horizontal current velocities were sampled from 5 to 38 m depth every 10 min by an RDI 600 kHz bottom-mounted ADCP in the vicinity of the buoy Nordseeboje 3 (NSB3, 54.68°N, 6.78°E) measurement station (Schultze et al. 2019). The ADCP data were used in the calculation of the bulk Richardson number.

Wind data

Wind velocities at 10 m height were obtained from measurements taken at 30 m height using the power law for wind profiles $w_{10} = w_{30}(z_{10}/z_{30})^{\alpha}$, where $\alpha = 1/7$, and w and z stand for the wind velocity at a given height, respectively (Hellmann 1919; Spera and Richards 1979). The subscripts denote estimates at 10 and 30 m.

Chl *a* fluorescence

The WET Labs FLNTU sensor measured Chl *a* fluorescence with excitation at 470 nm and emission recorded at 695 nm at a sampling rate of 1 Hz (Schultze et al. 2019). Spikes in the Chl *a* signal were identified and discarded by selecting a maximum noise threshold that corresponded to twice the 99th-percentile value of the complete data set. Daytime variations in Chl *a* fluorescence due to quenching were excluded by considering only nighttime measurements in the calculations, as well as in Fig. 2F.

Results

Stratification and turbulence before the storm events

Prior to the arrival of Storm Bertha to the study area at approximately 00:00 UTC on 09 August 2014, winds remained relatively low at levels below 6 Beaufort (i.e., < 10.8 m s^{-1}, Fig. 2A). During these pre-storm conditions, hereafter called

"background conditions," the water column consisted of a warm (~ 21°C) surface mixed layer separated from the cooler (~ 15°C) bottom mixed layer by a strongly stratified thermocline, characterized by sharp temperature gradients (Fig. 2B). We consider two thermocline definitions: the 80%-thermocline, which is characterized by the region of the water column at which 80% of the variation in temperature occurs and presents a mean $N^2 = 4.3 \times 10^{-3}$ s^{-2}; and the 90%-thermocline, which comprises 90% of the variation in temperature across the water column and has a mean $N^2 = 3.8 \times 10^{-3}$ s^{-2}. Unless specifically stated, we refer to the 90%-thermocline throughout this study.

During conditions of summer heating, both surface and bottom mixed layers form by being regularly mixed by turbulence arising from forcing at the boundaries of the water column: through wind and wave stresses at the water surface, and from friction between tidal currents and the sea-bed below. This turbulence can be seen in the glider-based measurements of the turbulent dissipation rate ε, in W kg^{-1}, which quantifies the strength of the turbulence (Fig. 2C). A regular cycle of turbulence was observed in the bottom layer at times corresponding to ebb and flood tides. More irregular episodes of higher turbulence (O[10^{-6} W kg^{-1}] – O[10^{-5} W kg^{-1}]) were present in the surface mixed layer coinciding with increased wind forcing.

The thermocline was characterized by much lower ε levels, which were on average seven times weaker than in the surface mixed layer, and displayed irregular bursts of high turbulence (O[10^{-6} W kg^{-1}]). The causes of this intermittent turbulence are thought to be associated with internal wave activity and enhanced shear due to inertial oscillations (Rippeth 2005; Burchard and Rippeth 2009). Despite the intermittent bursts of turbulence in the thermocline, the strong stratification damps mixed layer turbulence and limits the vertical fluxes of scalars across it. Stratification thus acts like a cap on the transport of nutrients, which Floeter et al. (2017) observed to have remained largely confined to the bottom mixed layer in 2014 (19–24 July) within 14–100 km distance from our study region. Moreover, the presence of a thermocline often leads to nutrient depleted conditions in the surface layer that limit an increase in phytoplankton biomass, and promotes the formation of a subsurface chlorophyll maximum (Ross and Sharples 2007), as seen in Fig. 2D. The difference in turbulence intensity between the thermocline, surface, and bottom mixed layers is shown through the histograms in Fig. 3A for the period before the storm.

Enhanced turbulence by the storm

The role of thermocline stratification in damping turbulence was altered with the arrival of Storm Bertha at approximately 00:00 UTC on 09 August, when elevated turbulence in the thermocline reached levels comparable to the surface and bottom mixed layers (Fig. 2C). The physical mechanism responsible for this change is revealed by examining time series of the dimensionless bulk Richardson number, $Ri_b = \Delta\rho g h/\rho_0(\Delta U)^2$, where $\Delta\rho$ and ΔU are the density and

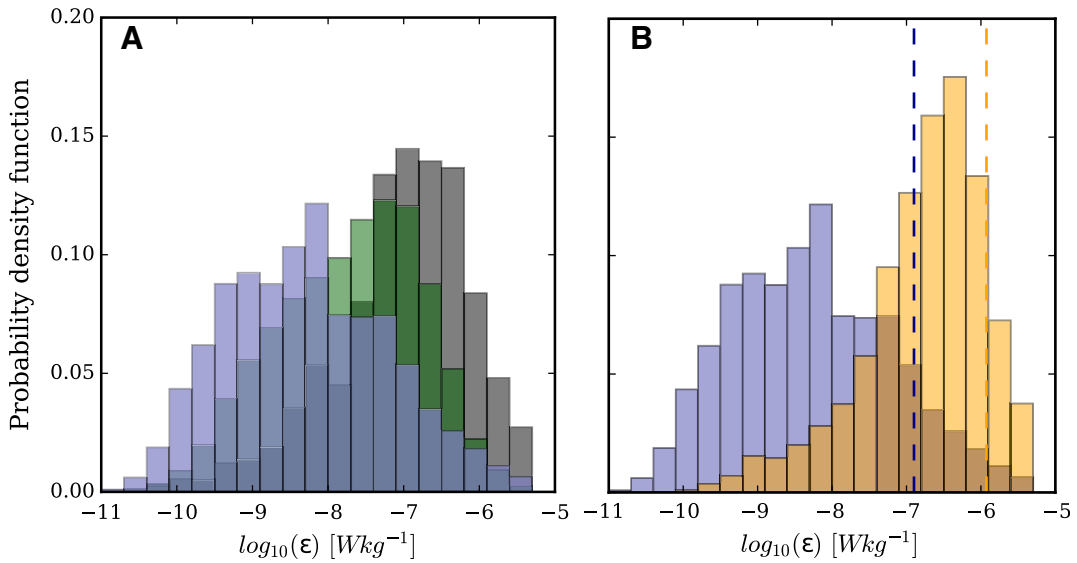

Fig. 3. (A) Probability density functions (PDFs) of the dissipation of turbulent kinetic energy in the surface mixed layer (black), bottom mixed layer (green), and thermocline (blue) during background conditions (06–09 August). (B) PDFs of the dissipation of turbulent kinetic energy within the thermocline before (blue) and during (orange) the periods of marginal stability. In the thermocline, the mean (median) ε before and during the marginal stability periods were 1.3×10^{-7} (5.0×10^{-9}) W kg^{-1} and 1.2×10^{-6} (2.5×10^{-7}) W kg^{-1}, respectively, whereby the mean of both regimes is indicated on the histogram by the dashed lines in the respective colors. In (A) and (B), transparency has been added to the PDFs to enable simultaneous visualization and comparison of the regimes.

velocity changes across the thermocline, ρ_0 is a representative water density, g the gravitational acceleration, and h denotes the thickness of the thermocline. Ri_b quantifies the relative importance of the destabilizing influence of shear, and the stabilizing influence of stratification. In pre-storm conditions, Fig. 2E shows that $Ri_b \gg 1$, indicating that stratification was relatively strong, and largely prevented the shear from generating turbulence (Schultze et al. 2017). However, as the wind forcing of the storm increased, periods of saturation with $Ri_b \approx 1/4$ were observed, a critical value in the stability of stratified shear layers, which we use as marks to characterize and quantify the anomalous storm conditions. Flows in which $Ri_b < 1/4$ are known to be unstable to the growth of Kelvin–Helmholtz instabilities, whereas $Ri_b > 1/4$ indicates stability (Smyth and Carpenter 2019). Thus, Fig. 2E shows that, independently of the thermocline definition considered, the storm drove the thermocline to a state of marginal stability on at least three occasions. At marginal stability, an intensification of the storm forcing causing increased ΔU led to a drop in Ri_b below the critical value, and the generation of shear instabilities that rapidly mixed the thermocline. This mixing increased the thermocline thickness, h, bringing it back to marginal stability. Thus, at marginal stability, any increase in the storm forcing led to direct increases in mixing the thermocline, whereas at larger Ri_b no such direct link was present. This creates a "mixing trigger" for enhanced storm-forced thermocline fluxes. Marginal stability has also been observed in a number of other forced, dissipative, stratified shear flows (Smyth and Moum 2013; Gargett et al. 2014).

Turbulence within the thermocline was altered during periods of storm-induced marginal stability. This is best seen in the distributions of ε shown in Fig. 3B, and quantified through the ratio of mean ε levels before and during the periods of marginal stability. Using the method described by Baker and Gibson (1987) for lognormally distributed variables, mean values of ε in the thermocline increased ninefold during these periods compared to pre-storm conditions (Figs. 2C and 3B). Moreover, the mean (median) ε during background conditions was 1.3×10^{-7} (6.4×10^{-9}) W kg^{-1} and raised to 1.2×10^{-6} (2.4×10^{-7}) W kg^{-1} in the marginal stability periods. Note that if the 80%-thermocline is considered, the mean turbulent flux during the marginal stability periods is a factor of 6 higher than under background conditions.

Mixing of stratification through enhanced turbulent flux across the thermocline

The enhanced turbulence within the thermocline led to a rapid destruction of the stratification through turbulent mixing. A quantitative measure of the strength of stratification is given by $\phi = (1/H)\int_0^H (\rho_{\mathrm{mix}} - \rho) g z \mathrm{d}z$, with the integral taken over the depth of the water column, H. Expressed in J m^{-3}, ϕ is the amount of potential energy contained in the stratification relative to the completely mixed state. This mixed state is characterized by a constant water density of $\rho_{\mathrm{mix}}(t) = \int_0^H \rho \mathrm{d}z/H$. Figure 2E shows that the greatest drops in ϕ coincided with the periods of marginal stability. In fact, from the onset of marginal stability at 01:30 UTC on 09 August, to the time of complete mixing shortly before 13 August, 71% of the total drop in stratification occurred during the three periods of marginal stability, with the remainder being mixed after the thermocline had descended well into the bottom boundary layer. These times of marginal stability also corresponded to drops in the temperature of the surface mixed layer (Fig. 2B) as a result of the increase in turbulent heat flux across the thermocline.

Response of Chl *a* to storm activity

As a means of assessing the biological response of this enhanced mixing, we examined glider-based in vivo measurements of Chl *a* fluorescence, expressed in relative units (Fig. 2D,F). Pre-storm conditions showed low Chl *a* in the surface mixed layer, consistent with low nutrient availability. However, with the passage of the storm, the in vivo fluorescence of Chl *a* in the surface mixed layer rose by 67%, achieving levels comparable to those in the thermocline and bottom mixed layer. While such a biological response is primarily related to a redistribution of phytoplankton cells over the water column, it is likely to be also linked to a net increase in Chl *a* and phytoplankton biomass. However, due to a myriad of influences affecting phytoplankton biomass (e.g., light and temperature dependence, predation), increased in vivo Chl *a* fluorescence cannot be readily associated with primary production without the support of direct measurements of biomass. Enhanced photosynthetic activity as a result of primary production is likely responsible for the observed increase in Chl *a* fluorescence over the water column (Falkowski and Kiefer 1985; Babin et al. 2004), however changes in the physiological status of the cells cannot be ruled out (Kiefer 1973; Falkowski and Kiefer 1985).

Discussion

The presented results show that storms are capable of changing the turbulent state of the thermocline in shelf seas through the formation of shear instabilities, implying a significantly enhanced turbulent flux from the cool and nutrient-rich bottom waters into the surface layer.

The intensification of turbulent fluxes can be quantified through the calculation of the buoyancy flux, $\mathscr{B} = \Gamma\varepsilon$, with the flux coefficient $\Gamma = 0.2$, consistent with previous studies in this field (Gregg et al. 2012, 2018; Schultze et al. 2017). Because vertical turbulent fluxes are directly proportional to ε, this results in a ninefold increase in the fluxes of important quantities such as heat and nutrients across the thermocline. A comparable increase has been observed through the calculation of a heat budget as an alternative means of estimating turbulent fluxes (not shown, see Schultze et al. 2017), which are in agreement with the turbulence measurements.

Although storms are known to episodically increase biological productivity (Babin et al. 2004; Walker et al. 2005; Rumyantseva et al. 2015), the importance of such extreme events on a seasonal basis is currently a matter of debate (Hanshaw et al. 2008; Foltz et al. 2015). In our study, thermocline fluxes were observed to increase ninefold during the 29 h of marginal stability, which corresponds to a total amount of turbulent fluxes that would otherwise have been obtained over 11 d under normal background conditions.

Seasonal relevance of storm events on turbulent fluxes

The rapid mixing of a strongly stratified water column triggered by one storm event raises questions about the seasonal importance of summer storms. Aiming at providing a rough, order-of-magnitude estimate for summer storms, we consider the mean duration of the stratified season in the German Bight of the North Sea of 85 d (van Leeuwen et al. 2015; Carpenter et al. 2016), which occurs during a representative summer that consists of 123 d (from the beginning of May until the end of August). Therefore, in the following analysis, the study region is considered to be stratified 69% of the time during summer.

From an analysis of the wind speed measurements at the FINO 3 offshore platform from the years 2010 to 2016, we are able to assess the relative occurrence of summer storm events, which we define as wind speeds of Beaufort 6 and higher, that is, greater than 10.8 m s^{-1}. This strength of wind forcing was shown in Fig. 2 to be sufficient to initiate marginal stability in the thermocline during conditions of strong stratification. The FINO 3 data set shows that an average of 8.3 d (200 h) of storm events occur per summer season. Assuming that a similar fraction of time is spent at marginal stability (67%) and a coincident increase in turbulent thermocline fluxes by a factor of 9, as observed during Storm Bertha, this leads to the equivalent of 35 d of storm-induced fluxes at background stratified levels, corresponding to 40% of the total thermocline fluxes in summer. Note that even if the 80%-thermocline is considered, storms are responsible for 27% of the total fluxes across the stratified water column following the same argumentation. These rough estimates indicate that, during the stratified season, net storm-induced turbulent fluxes could be comparable to the net background flux, and act as a significant supply of nutrients to the depleted surface mixed layer during the summer growing season.

Due to the large number of uncertainties associated with this analysis, such as dependencies on wind speeds and stratification levels, we stress the need to further investigate the importance of turbulent fluxes generated by storm events from a seasonal perspective. Other uncertainties that should be tackled in future studies would be the notion that a storm is connected to wind speeds greater than 10.8 ms^{-1} and the related onset of marginal stability. In addition, we have neglected increases in storm-driven mixing that take place outside of the periods of marginal stability and hence elevated wind speeds. This could also have an influence in increasing storm-driven fluxes (Rippeth et al. 2005; Rumyantseva et al. 2015), as seen at the end of the last marginal stability period in Fig. 2E. Despite these uncertainties, we have provided with this analysis an order-of-magnitude estimate that highlights the potential importance of storms in providing a significant fraction of seasonal fluxes on the North Sea shelf, a topic that should be further investigated in future studies.

References

Babin, S. M., J. A. Carton, T. D. Dickey, and J. D. Wiggert. 2004. Satellite evidence of hurricane-induced phytoplankton blooms in an oceanic desert. J. Geophys. Res. Oceans: 109. doi:10.1029/2003JC001938

Baker, M. A., and C. H. Gibson. 1987. Sampling turbulence in the stratified ocean: Statistical consequences of strong intermittency. J. Phys. Oceanogr. **17**: 1817–1836. doi:10.1175/1520-0485(1987)017<1817:STITSO>2.0.CO;2

Burchard, H., and T. P. Rippeth. 2009. Generation of bulk shear spikes in shallow stratified tidal seas. J. Phys. Oceanogr. **39**: 969–985. doi:10.1175/2008JPO4074.1

Carpenter, J. R., L. Merckelbach, U. Callies, S. Clark, L. Gaslikova, and B. Baschek. 2016. Potential impacts of offshore wind farms on North Sea stratification. PLoS One **11**: e0160830. doi:10.1371/journal.pone.0160830

Falkowski, P., and D. A. Kiefer. 1985. Chlorophyll a fluorescence in phytopankton: Relationship to photosynthesis and biomass. J. Plankton Res. **7**: 715–731. doi:10.1093/plankt/7.5.715

Fer, I., A. K. Peterson, and J. E. Ullgren. 2014. Microstructure measurements from an underwater glider in the turbulent Faroe Bank Channel overflow. J. Atmos. Oceanic Tech. **31**: 1128–1150. doi:10.1175/JTECH-D-13-00221.1

Feser, F., M. Barcikowska, O. Krueger, F. Schenk, R. Weisse, and L. Xia. 2015. Storminess over the North Atlantic and northwestern Europe—a review. Q. J. Roy. Meteorol. Soc. **141**: 350–382. doi:10.1002/qj.2364

Floeter, J., and others. 2017. Pelagic effects of offshore wind farm foundations in the stratified North Sea. Prog. Oceanogr. **156**: 154–173. doi:10.1016/j.pocean.2017.07.003

Foltz, G. R., K. Balaguru, and L. R. Leung. 2015. A reassessment of the integrated impact of tropical cyclones on surface chlorophyll in the western subtropical North Atlantic. Geophys. Res. Lett. **42**: 1158–1164. doi:10.1002/2015GL063222

Gargett, A., D. Savidge, and J. Wells. 2014. Anatomy of a langmuir supercell event. J. Mar. Res. **72**: 127–163. doi:10.1357/002224014814901976

Glenn, S. M., and others. 2016. Stratified coastal ocean interactions with tropical cyclones. Nat. Commun. **7**: 10887. doi:10.1038/ncomms10887

Gregg, M., E. D'Asaro, J. Riley, and E. Kunze. 2018. Mixing efficiency in the ocean. Ann. Rev. Mar. Sci. **10**: 443–473. doi:10.1146/annurev-marine-121916-063643

Gregg, M. C., M. H. Alford, H. Kontoyiannis, V. Zervakis, and D. Winkel. 2012. Mixing over the steep side of the Cycladic plateau in the Aegean Sea. J. Mar. Syst. **89**: 30–47. doi:10.1016/j.jmarsys.2011.07.009

Hanshaw, M. N., M. S. Lozier, and J. B. Palter. 2008. Integrated impact of tropical cyclones on sea surface chlorophyll in the North Atlantic. Geophys. Res. Lett. **35**: L01601. doi:10.1029/2007GL031862

Hellmann, G. 1919. Über die Bewegung der Luft in den untersten Schichten der Atmosphäre, Kgl. Akademie der Wissenschaften [G.] Reimer.

Kiefer, D. A. 1973. Chlorophyll a fluorescence in marine diatoms: Response of chloroplasts to light and nutrient stress. Mar. Biol. **23**: 39–46. doi:10.1007/BF00394110

Lueck, R. G., F. Wolk, and H. Yamazaki. 2002. Oceanic velocity microstucture measurements in the 20th century. J. Oceanogr. **58**: 153–174. doi:10.1023/A:1015837020019

Rippeth, T. P. 2005. Mixing in seasonally stratified shelf seas: A shifting paradigm. Philos. Trans. A. Math. Phys. Eng. Sci. **363**: 2837–2854. doi:10.1098/rsta.2005.1662

Rippeth, T. P., M. R. Palmer, J. H. Simpson, N. R. Fisher, and J. Sharples. 2005. Thermocline mixing in summer stratified continental shelf seas. Geophys. Res. Lett. **32**: L05602. doi:10.1029/2004GL022104

Ross, O. N., and J. Sharples. 2007. Phytoplankton motility and the competition for nutrients in the thermocline. Mar. Ecol. Prog. Ser. **347**: 21–38. doi:10.3354/meps06999

Rumyantseva, A., N. Lucas, T. Rippeth, A. Martin, S. C. Painter, T. J. Boyd, and S. Henson. 2015. Ocean nutrient pathways associated with the passage of a storm. Global Biogeochem. Cycles **29**: 1179–1189. doi:10.1002/2015GB005097

Schultze, L. K. P., L. M. Merckelbach, and J. R. Carpenter. 2017. Turbulence and mixing in a shallow shelf sea from underwater gliders. J. Geophys. Res. Oceans **122**: 9092–9109. doi:10.1002/2017JC012872

Schultze, L. K. P., L. M. Merckelbach, and J. R. Carpenter. 2019. Glider, turbulence and ADCP datasets used in the manuscript "Storm-induced turbulence alters shelf sea vertical fluxes". doi:10.5281/zenodo.3525787

Simpson, J., and J. Sharples. 2012, *Introduction to the physical and biological oceanography of shelf seas*. Cambridge Univ. Press.

Smyth, W. D., and J. R. Carpenter. 2019, *Instability in geophysical flows*. Cambridge Univ. Press. doi:10.1364/AO.58.008802

Smyth, W. D., and J. N. Moum. 2013. Marginal instability and deep cycle turbulence in the eastern equatorial Pacific Ocean. Geophys. Res. Lett. **40**: 6181–6185. doi:10.1002/2013GL058403

Spera, D. A., and T. R. Richards. 1979. Modified power law equations for vertical wind profiles, in: Wind Energy Charact. Wind Energy Siting, Portland. doi:10.3109/01485017908987335

Thomas, H., Y. Bozec, K. Elkalay, and H. J. W. de Baar. 2004. Enhanced open ocean storage of CO_2 from shelf sea pumping. Science **304**: 1005–1008. doi:10.1126/science.1095491

van Beusekom, J. E., and S. Diel-Christiansen. 2009. Global change and the biogeochemistry of the North Sea: The possible role of phytoplankton and phytoplankton grazing. Int. J. Earth Sci. **98**: 269–280. doi:10.1007/s00531-007-0233-8

van Leeuwen, S., P. Tett, D. Mills, and J. van der Molen. 2015. Stratified and nonstratified areas in the North Sea: Long-term variability and biological and policy implications. J. Geophys. Res. Oceans **120**: 4670–4686. doi:10.1002/2014JC010485

Walker, N. D., R. R. Leben, and S. Balasubramanian. 2005. Hurricane-forced upwelling and chlorophyll a enhancement within cold-core cyclones in the Gulf of Mexico. Geophys. Res. Lett. **32**: L18610. doi:10.1029/2005GL023716

Wolk, F., H. Yamazaki, L. Seuront, and R. G. Lueck. 2002. A new free-fall profiler for measuring biophysical microstructure. J. Atmos. Oceanic Tech. **19**: 780–793. doi:10.1175/1520-0426(2002)019<0780:ANFFPF>2.0.CO;2

Acknowledgments

We would like to acknowledge B. Baschek, Y. Voynova, and J.-P. Mellado for helpful discussions. Support for the preparation, deployment, and recovery of instrumentation were provided by R. Kopetzky, B. Peters, A. Werner, M. Heineke, and the captain and crew of the *RV Ludwig Prandtl*. Funding was provided through the Polar Regions and Coasts in the Changing Earth System (PACES II) program of the Helmholtz Association. We would like to acknowledge the German Federal Ministry of Economic Affairs and Energy (BMWi) and the Project Management Jülich (PTJ), which made the wind measurements of the platform Fino 3 available for use. We also thank the German Federal Maritime and Hydrographic Agency (BSH) for their support in deploying and recovering the ADCP. This paper is a contribution to the project T2 of the Collaborative Research Centre TRR181, "Energy Transfer in Atmosphere and Ocean."

A more detailed discussion of the methodology can be found in Spera and Richards (1979), Lueck et al. (2002), Wolk et al. (2002), and Gregg et al. (2012).

Submitted 29 May 2019
Revised 16 November 2019
Accepted 12 December 2019